THE JOURNAL OF BIOLOGICAL CHEMISTRY VOL. 289, NO. 52, pp. 36116–36124, December 26, 2014


# Amino Acid Residues 489–503 of Dihydropyridine Receptor (DHPR) $\beta_{1a}$ Subunit Are Critical for Structural Communication between the Skeletal Muscle DHPR Complex and Type 1 Ryanodine Receptor*

Received for publication, September 29, 2014, and in revised form, October 31, 2014 Published, JBC Papers in Press, November 10, 2014, DOI 10.1074/jbc.M114.615526

**Jose M. Eltit**[‡], **Clara Franzini-Armstrong**[§], **and Claudio F. Perez**[¶1]

*From the* [¶]*Department of Anesthesiology Perioperative and Pain Medicine, Brigham and Women's Hospital, Harvard Medical School, Boston, Massachusetts 02115, the* [‡]*Department of Physiology and Biophysics, School of Medicine, Virginia Commonwealth University, Richmond, Virgina 23298, and the* [§]*Department of Cell and Developmental Biology, University of Pennsylvania, Philadelphia, Pennsylvania 19104*

**Background:** Dihydropyridine receptor (DHPR) $\beta_{1a}$ subunit is essential for muscle contraction.
**Results:** Deletion of residues 489–503 in the $\beta_{1a}$ C terminus prevents calcium signaling and DHPR tetrad formation.
**Conclusion:** $\beta_{1a}$ C terminus is critical for structural communication with the $Ca^{2+}$ release channel.
**Significance:** The $\beta_{1a}$ C-terminal tail is as important as the DHPR $\alpha_{1S}$ II–III loop for skeletal EC coupling.

**The $\beta_{1a}$ subunit is a cytoplasmic component of the dihydropyridine receptor (DHPR) complex that plays an essential role in skeletal muscle excitation-contraction (EC) coupling. Here we investigate the role of the C-terminal end of this auxiliary subunit in the functional and structural communication between the DHPR and the $Ca^{2+}$ release channel (RyR1). Progressive truncation of the $\beta_{1a}$ C terminus showed that deletion of amino acid residues $Gln^{489}$ to $Trp^{503}$ resulted in a loss of depolarization-induced $Ca^{2+}$ release, a severe reduction of L-type $Ca^{2+}$ currents, and a lack of tetrad formation as evaluated by freeze-fracture analysis. However, deletion of this domain did not affect expression/targeting or density ($Q_{max}$) of the DHPR-$\alpha_{1S}$ subunit to the plasma membrane. Within this motif, triple alanine substitution of residues $Leu^{496}$, $Leu^{500}$, and $Trp^{503}$, which are thought to mediate direct $\beta_{1a}$-RyR1 interactions, weakened EC coupling but did not replicate the truncated phenotype. Therefore, these data demonstrate that an amino acid segment encompassing sequence $^{489}$QVQVLTSLRRNLSFW$^{503}$ of $\beta_{1a}$ contains critical determinant(s) for the physical link of DHPR and RyR1, further confirming a direct correspondence between DHPR positioning and DHPR/RyR functional interactions. In addition, our data strongly suggest that the motif $Leu^{496}$-$Leu^{500}$-$Trp^{503}$ within the $\beta_{1a}$ C-terminal tail plays a nonessential role in the bidirectional DHPR/RyR1 signaling that supports skeletal-type EC coupling.**

Excitation-contraction (EC)[2] coupling in skeletal muscle involves a direct interaction between the L-type $Ca^{2+}$ channel, 1–4-dihydropyridine receptor (DHPR) complex, located in the surface membrane and the type 1 ryanodine receptor (RyR1), $Ca^{2+}$ release channel in the sarcoplasmic reticulum (SR) membrane (1–3). This interaction does not require $Ca^{2+}$ permeation through the DHPR but instead relies on direct reciprocal communication between the two channels. Although there is compelling supporting evidence that both the DHPR-$\alpha_{1S}$ (Cav1.1) and DHPR-$\beta_{1a}$ (Cav$\beta$1) subunits are essential components for the DHPR/RyR1 communication (4–11), the mechanisms by which conformational changes of the DHPR complex translate into activation of RyR1 during skeletal EC coupling remain unclear.

Structure/function studies in cultured myotubes have revealed that the cytosolic loop linking repeats II and III (the II–III loop) of the DHPR-$\alpha_{1S}$ subunit plays an essential role in the bidirectional signaling with RyR1. Within this intracellular loop, residues 720–765 are critical to support both depolarization-induced $Ca^{2+}$ release, also known as the orthograde signal (1, 12, 13), and the ability of the DHPR complex to receive a retrograde activation signal from RyR1 (1, 14). Importantly, the same region is also required to support the stereospecific positioning of DHPR complexes in relation to RyR1 that result in the assembly of ordered DHPR tetrad arrays characteristic of skeletal muscle (15).

The role of the DHPR-$\beta_{1a}$ subunit in skeletal EC coupling stems from studies in $\beta_1$-null mice showing that a lack of $\beta_{1a}$ expression eliminates electrically evoked $Ca^{2+}$ release from the SR (9). Most revealing are recent observations on the paralyzed zebrafish mutant *relaxed* that lacks expression of the DHPR-$\beta_{1a}$ subunit. In muscle fibers from this fish model, the DHPR complex, although reduced in number, is appropriately targeted to the junctional SR but is not arranged in tetrads (16, 17). These studies confirm that functional skeletal-type EC coupling requires the appropriate alignment of DHPRs with RyR1 and strongly suggest that the $\beta_{1a}$ subunit is essential in this positioning. It is currently unclear whether the $\beta_{1a}$ subunit is additionally involved in transmitting the activation signal from

* This work was supported, in whole or in part, by National Institutes of Health Grants R03AR066359 (to C. F. P.) and R01 HL48093 and 2P01AR052354 (to C. F. A.). This work was also supported by fund from the William S. Milton Fund/Harvard Medical School (to C. F. P.).
[1] To whom correspondence should be addressed: Dept. of Anesthesiology Perioperative and Pain Medicine. Brigham and Women's Hospital, 20 Shattuck St., Boston, MA 02115. Tel.: 617-525-6486; Fax: 617-732-6927; E-mail: cperez@zeus.bwh.harvard.edu.
[2] The abbreviations used are: EC, excitation-contraction; DHPR, 1–4-dihydropyridine receptor; RyR1, type 1 ryanodine receptor; SR, sarcoplasmic reticulum; F, fluorescence; SH, Src homology.

the DHPR to RyR1 and/or directly modulating RyR1 function. Studies on chimeric $\beta_{2a}/\beta_{1a}$ and truncated $\beta_{1a}$ subunits have shown that deletion, or substitution, of 35 residues within the $\beta_{1a}$ C-terminal end produces a severe reduction in voltage-evoked $Ca^{2+}$ transient amplitude and DHPR $Ca^{2+}$ current density (18, 19), suggesting a critical contribution of the $\beta_{1a}$ C-terminal tail to skeletal-type EC coupling signaling. However, because no structural information was obtained in these studies, it is unclear whether the effects of $\beta_{1a}$ in EC coupling are simply due to an effect on DHPR positioning. Recent *in vitro* studies have shown that peptides fragments from the C-terminal domain of $\beta_{1a}$ modulate RyR1 channel function, giving support to the idea of a direct functional interaction between $\beta_{1a}$ and RyR1 (20). Mutational analysis of these peptides identified the critical motif responsible for RyR1 activation in a hydrophobic pocket formed by amino acid residues $Leu^{496}$-$Leu^{500}$-$Trp^{503}$ (21). However, it is currently unknown whether the alleged $\beta_{1a}$-RyR1 interaction mediated by this motif plays any role either in the bidirectional signaling between RyR1 and DHPR or in the DHPR/RyR1 physical linkage that supports DHPR tetrad arrays.

In this study, we examine these questions by assessing the effect on EC coupling signaling of deletions and mutations of the amino acid sequence within the $Leu^{496}$-$Leu^{500}$-$Trp^{503}$ hydrophobic pocket of mouse $\beta_{1a}$ subunit. We find that progressive truncations of $\beta_{1a}$ C-terminal tail significantly affected depolarization-induced $Ca^{2+}$ release, retrograde signaling, and the arrangement of DHPR into tetrads. Moreover, although the disruption of motif $Leu^{496}$-$Leu^{500}$-$Trp^{503}$ weakened EC coupling, it did not prevent bidirectional signaling or DHPR tetrad formation. In summary, our data again establish a direct correspondence between DHPR positioning and DHPR/RyR functional interactions, revealing a key role for amino acid sequence $Gln^{489}$–$Trp^{503}$ in this process. In addition, our data indicate that although the $Leu^{496}$-$Leu^{500}$-$Trp^{503}$ motif contributes to normal bidirectional communication between the DHPR and RyR1, it does not appear to constitute a critical determinant for skeletal EC coupling.

## EXPERIMENTAL PROCEDURES

*cDNA Constructs and Virus Packaging*—Full-length cDNA of mouse $\beta_{1a}$ subunit (GenBank™, NM_031173), as well as the $\beta_{1a}$ truncated constructs, were cloned into a retroviral vector by inserting the AgeI-NotI cloning cassette from vector pSG5T7-AgeNot$\beta_{1a}$ (gift from Dr. R. Coronado) into the corresponding restriction sites of the bicistronic retroviral vector pCMMP-MCS-IRES-Puro carrying a Puromycin resistance gene (Addgene 36952 (22)). Truncation of the C-terminal tail of $\beta_{1a}$ subunit was performed by inserting a set of two complementary oligonucleotide primers containing the desired truncated sequence in frame into pSG5T7-AgeNot$\beta_{1a}$ within restriction sites BsmBI and NotI (for $\beta_{-21}$, $\beta_{-36}$, and $\beta_{LLW}$ mutant clones) or SacII and NotI (for $\beta_{-14}$). A stop codon was engineered at the 3′ end of each primer upstream of the NotI site. All clones were confirmed by sequencing prior to use. Details of the deleted sequence and mutated residues of the clones analyzed in this study are summarized in Fig. 1. Virus production was performed with a set of three packaging vectors as described elsewhere (23).

*Cell Culture and Calcium Imaging*—Primary myoblasts from $\beta_1$-null muscles (5, 9) infected with $\beta_{1a}$ cDNA-containing virions at a multiplicity of infection of 0.5 were selected with 1.5 $\mu$g/ml Puromycin for 2 weeks to obtain stably transduced myoblasts. $\beta_1$-Expressing myoblasts were then grown and differentiated in 96-well plates as described previously (24). Calcium imaging was performed 4–5 days after differentiation in myotubes loaded with 5 $\mu$M Fura2-AM (Molecular Probes, OR) in imaging buffer (125 mM NaCl, 5 mM KCl, 2 mM $CaCl_2$, 1.2 mM $MgSO_4$, 6 mM glucose, and 25 mM Hepes/Tris, pH 7.4). Membrane depolarization was performed by a 5-s perfusion with 5–7 volumes of imaging buffer containing increased concentrations of KCl supplemented with or without 0.5 mM $CdCl_2$ and 0.1 mM $LaCl_3$. To preserve osmolarity of the depolarization buffer, the increased $K^+$ concentration was compensated with an equivalent reduction in total NaCl concentration. Cells were imaged with an intensified 10-bit digital CCD camera (XR-Mega-10; Stanford Photonics, Stanford, CA) using a DG4 multiwavelength light source. Fluorescent emission at 510 nm was captured from regions of interest within each myotube at 33 frames per second using Piper-controlled acquisition software (Stanford Photonics) and expressed as ratio of signal collected at alternating 340/380-nm excitation wavelength.

*Immunofluorescence Labeling*—Myotubes were differentiated in $\mu$-Slide microscopy chambers (Ibidi®) and fixed with either 4% paraformaldehyde/PBS solution or cold methanol (−20 °C) for 15 min. The cells were then washed, permeabilized (if applicable), and immunostained with anti-DHPR $\alpha_{1S}$ monoclonal antibody MA3–921 (Thermo Scientific, Rockford, IL) or anti-DHPR $\beta_{1a}$ monoclonal antibody N7/18 (Neuromab; UC Davis). The images were obtained on an Olympus IX70 microscope using a SPOT/RT3 digital camera (Diagnostic Instruments Inc.) and processed with Adobe® Photoshop CS3 (version 10.0.1).

*Freeze Fracture Replicas*—The cells were grown and differentiated on Thermanox™ coverslips (Nunc Inc., Naperville, IL) coated with extracellular matrix gel (25). Differentiated myotubes were washed twice in PBS at 37 °C, fixed in 3.5% glutaraldehyde in 100 mM sodium cacodylate buffer (pH 7.2), and then infiltrated with 30% glycerol, frozen, and fractured as described previously (15, 26). Association of particles with RyR1 orthogonal arrays and frequency of tetrad formation were assessed as described (15, 27). For each truncated construct, we used digitized images from micrographs taken at a magnification of 33,900× and selected clusters that were most highly populated with particles and showed most evidence for order. We further limited the measurements within each cluster to areas that had either coherent arrays of tetrads with the same orientation or an evenly distributed set of particles. The density of DHPR particles at the peripheral coupling of each tested construct was estimated by counting all large particles that are clearly clustered and located over slightly raised mounds, which represent the peripheral coupling site.

*Measurement of Ionic Currents*—Macroscopic $Ca^{2+}$ currents were measured using the whole cell patch clamp technique according to previously described protocols (28). Myotubes

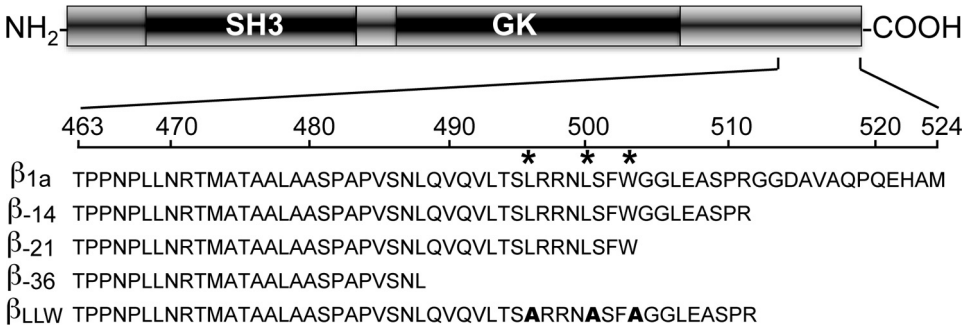


FIGURE 1. **Amino acid sequence alignment of $\beta_{1a}$ C-terminal region.** *Boxes* indicate relative position of conserved (SH3, GK) and variable (*light gray*) domains of the $\beta_{1a}$ subunit. Sequence alignment shows the $\beta_{1a}$ C-terminal truncations in each of the indicated clones. *Asterisks* indicate the locations of amino acid residues Leu$^{496}$, Leu$^{500}$, and Trp$^{503}$ that were mutated to alanine in clone $\beta_{LLW}$ (*bold letters*).

were voltage-clamped with the use of an Axopatch 200B amplifier (Axon Instruments, Foster City, CA). Effective series resistance was compensated up to the point of amplifier oscillation with the Axopatch circuit, and the leak current was subtracted by using a -P/6 protocol before each sweep. The patch pipettes were coated using Sylgard and had a resistance of ~2 MΩ when filled with the pipette solution. The patch pipette internal solution consisted of 140 mM cesium aspartate, 5 mM $MgCl_2$, 10 mM Cs-EGTA, and 10 mM Hepes titrated with CsOH to pH 7.2. The composition of the external bath solution was 145 mM TEA-Cl, 10 mM $CaCl_2$, 10 mM Hepes titrated with TEA(OH) to pH 7.4.

Intramembrane charge movement was determined following the protocol described previously (29). The internal and external pipette solutions had the same ionic composition described above. However, the external solution was supplemented with 0.5 mM $CdCl_2$ and 0.1 mM $LaCl_3$ to block L-type $Ca^{2+}$ currents. A 1-s prepulse to −30 mV to inactivate both sodium and transient calcium channels preceded the test pulses. The leak current and other passive components of the total current was subtracted by using a -P/6 protocol before each sweep. The patch pipettes were Sylgard-coated and had a tip resistance of 1.5–2.0 MΩ when filled with the internal solution. The serial resistance was corrected to 70% using the Axopath circuit with cell capacitance <100 pF in most recordings. The recorded signal was filtered to 5 kHz and was digitalized at 20 kHz. All experiments were performed at room temperature.

The voltage dependence of the $Ca^{2+}$ currents was fitted to the following equation,

$$I = G_{max}(V - V_r)/[1 + \exp((V_{1/2} - V)/k)] \quad \text{(Eq. 1)}$$

where $G_{max}$ is the maximal conductance, $V$ corresponds to the test potentials, $V_{1/2}$ is the potential at which $G = 1/2\ G_{max}$. $k$ represents a slope parameter, and $V_r$ is the reversion potential.

The voltage dependence of the charge movement was fitted to the following equation,

$$Q_{on} = Q_{max}/[1 + \exp((V_{1/2} - V)/k)] \quad \text{(Eq. 2)}$$

where $Q_{max}$ is the maximal charge, $V$ corresponds to the test potentials, $V_{1/2}$ is the potential at which $Q = 1/2\ Q_{max}$, and $k$ represents a slope parameter.

*Data Analysis*—Statistical significant differences among data sets were calculated using one-way analysis of variance (GraphPad Software, San Diego, CA). The data were expressed as means ± S.D. or means ± S.E.

## RESULTS

*C-terminal Truncation of $\beta_{1a}$ Does Not Affect Targeting of $\alpha_{1S}$ Subunit to the Plasma Membrane*—To assess the role of the C-terminal domain of the $\beta_{1a}$ subunit in skeletal-type EC coupling, we constructed a series of truncated DHPR-$\beta_{1a}$ subunits bearing progressive deletions of its C-terminal tail (Fig. 1) and then confirmed their expression and ability to target the DHPR complex to the surface membrane using immunocytochemical analysis (Fig. 2). No $\beta_{1a}$ or $\alpha_{1S}$ expression was detected in $\beta_1$-null myotubes (Fig. 2, *A* and *B*). In contrast, expression of wild type $\beta_{1a}$ in these myotubes restored proper targeting of the $\alpha_{1S}$ subunit to the surface membrane in discrete foci sometimes organized in a semilinear longitudinal orientation (Fig. 2, *C* and *D*). Because myotubes at this stage of differentiation have few internal $Ca^{2+}$ release units, most of the foci represent peripheral couplings where the SR cisternae bind the plasmmalema. Overall, immunocytochemistry revealed no obvious differences in expression and distribution of the $\beta_{1a}$ constructs used in this study (Fig. 2, *E–L*). Noticeably, the $\beta_{1a}$ truncations that support skeletal EC coupling signaling (see below) displayed the same clustered distribution pattern of $\alpha_{1S}$ and $\beta_{1a}$ expression as those that diminish or prevent EC coupling.

*Progressive Truncation of the $\beta_{1a}$ C-terminal Tail Impairs Depolarization-induced $Ca^{2+}$ Release*—The role of the $\beta_{1a}$ C-terminal tail in skeletal EC coupling was evaluated by comparing the effect of each truncation on depolarization-induced $Ca^{2+}$ release signals (Fig. 3). Calcium release was estimated from the average peak of the $Ca^{2+}$ transient of Fura2-loaded myotubes depolarized with increased $K^+$ concentrations. Calcium signals were measured either in the presence of $Cd^{2+}$ and $La^{3+}$ in nominal free $Ca^{2+}$ to measure skeletal-type EC coupling, which depends entirely on the direct DHPR-RyR interaction (Fig. 3*A*), or in the presence of 2 mM $CaCl_2$ (Fig. 3*B*). In the presence of $Cd^{2+}$ and $La^{3+}$, $Ca^{2+}$ transients measured from $\beta_{1a}$-expressing myotubes displayed a classic sigmoidal $K^+$ dose-response curves. (Fig. 3, *black circles*). The average peak amplitude of the $Ca^{2+}$ transients for clone $\beta_{-14}$ (lacking 14 amino acids of the C-terminal tail) were quite similar to those restored by $\beta_{1a}$ (Fig. 3*A*). Construct $\beta_{-21}$ (lacking 21 amino acids of the C-terminal tail) induced a small but statistically

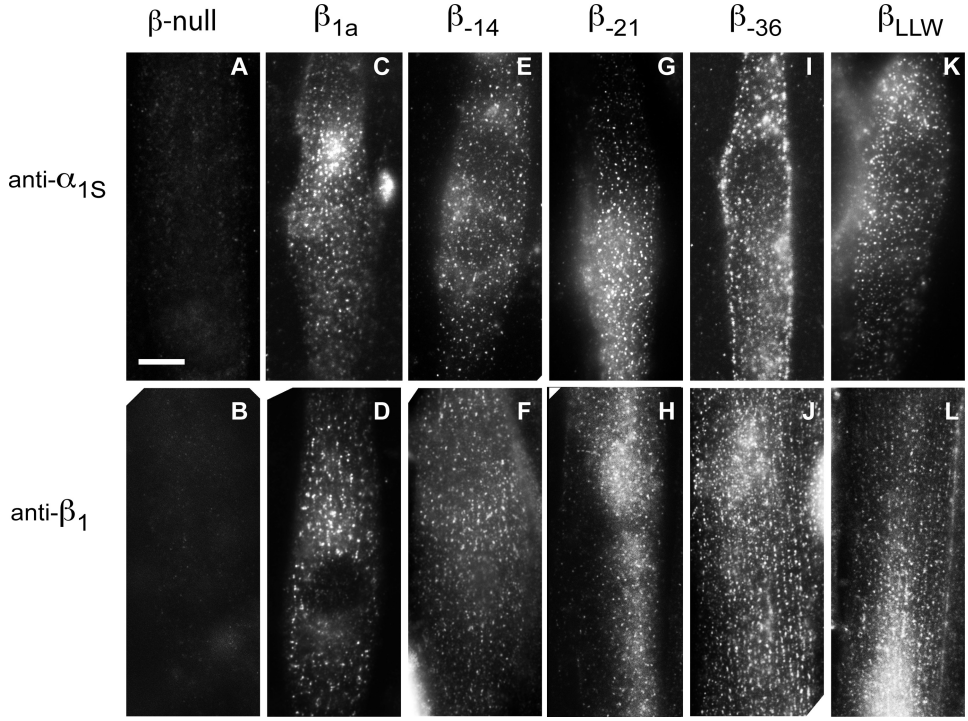


FIGURE 2. **C-terminal truncations of $\beta_{1a}$ subunit do not affect expression/targeting of the DHPR complex.** Representative inmunostaining pattern of expression of DHPR-$\alpha_{1S}$ (*A*, *C*, *E*, *G*, *I*, and *K*) and DHPR-$\beta_{1a}$ subunits (*B*, *D*, *F*, *H*, *J*, and *L*) of $\beta_1$-null myotubes expressing wild type and truncated $\beta_{1a}$ subunits. Pictures show a focal plane near the surface of the myotubes. *Bar*, 10 $\mu$m.

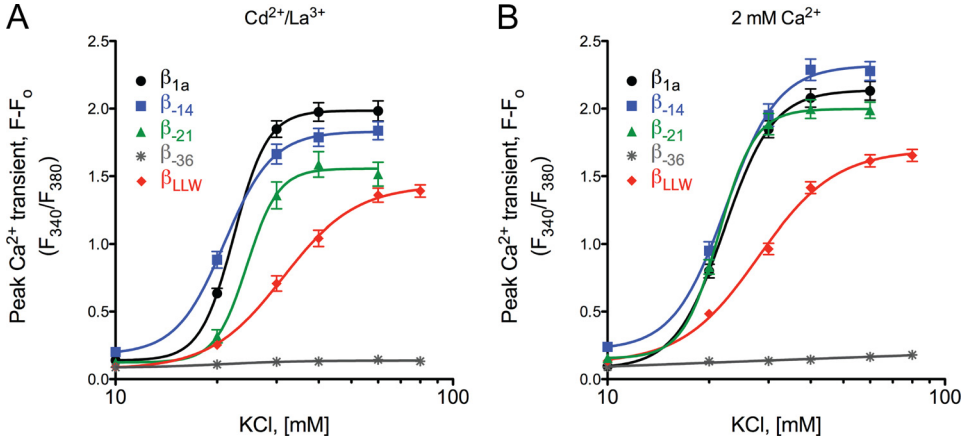


FIGURE 3. **Truncation of $\beta_{1a}$ C terminus prevents skeletal-type EC coupling.** Average peak $Ca^{2+}$ transient amplitude induced by depolarization of $\beta_1$-null myotubes expressing wild type $\beta_{1a}$ (*black circles*), $\beta_{-14}$ (*blue squares*), $\beta_{-21}$ (*green triangles*), $\beta_{-36}$ (*gray asterisks*), or $\beta_{LLW}$ subunit (*red diamonds*). Myotubes were loaded with 5 $\mu$M Fura-2 and exposed to the indicated concentrations of $K^+$ for 5 s in either $Cd^{2+}$ and $La^{3+}$ and no added $Ca^{2+}$ (*A*) or 2 mM $Ca^{2+}$ (*B*). The data are expressed as means ± S.E. for a total of 30–68 individual myotubes ($n = 3$) and fitted to a sigmoidal dose-response curve with variable slope. Fitting parameters are summarized in Table 1.

**TABLE 1**

**Average $K^+$ $EC_{50}$ and peak $Ca^{2+}$ transient at 60 mM $K^+$ depolarization**

The values are the means ± S.E.

| Construct | $K^+$ $EC_{50}$ (*n*) | | Peak $Ca^{2+}$ transient | |
|---|---|---|---|---|
| | 2 mM $Ca^{2+}$ | $Cd^{2+}/La^{3+}$ | 2 mM $Ca^{2+}$ | $Cd^{2+}/La^{3+}$ |
| | *mM* | | *mM* | |
| $\beta_{1a}$ | 21 ± 3 (30) | 22 ± 2 (35) | 2.13 ± 0.34 | 1.95 ± 0.34 |
| $\beta_{-14}$ | 24 ± 4 (42) | 23 ± 5 (68) | 2.28 ± 0.46 | 1.84 ± 0.54 |
| $\beta_{-21}$ | 22 ± 4 (31) | 25 ± 4 (27) | 1.99 ± 0.36 | 1.52 ± 0.46[a] |
| $\beta_{-36}$ | NA[b] | NA | 0.17 ± 0.04[a] | 0.14 ± 0.04[a] |
| $\beta_{LLW}$ | 29 ± 4[a] (34) | 33 ± 7[a] (52) | 1.61 ± 0.34[a] | 1.36 ± 0.38[a] |

[a] $p < 0.001$, compared with $\beta_{1a}$, one-way analysis of variance (Tukey's test).
[b] NA, not applicable.

significant reduction in the peak $Ca^{2+}$ transient amplitude, from a maximum 340/380 ratio of 1.95 ± 0.34 in $\beta_{1a}$ to 1.52 ± 0.46 in $\beta_{-21}$ (approximately 22% reduction; Table 1) without a change in sensitivity to depolarization. The construct $\beta_{-36}$ (lacking 36 amino acids of the C-terminal tail) elicited a severe disruption of the $Ca^{2+}$ signal rendering myotubes unresponsive to depolarization (Fig. 3, *gray asterisks*). On the other hand, in the presence of 2 mM extracellular $Ca^{2+}$, both $\beta_{-14}$ and $\beta_{-21}$ constructs restored the $Ca^{2+}$ transient peak to wild type levels (Fig. 3*B* and Table 1). However, myotubes expressing $\beta_{-36}$ did not respond to $K^+$ treatment even in the presence of extracellular $Ca^{2+}$. This is not due to a lack of expression or mistargeting of either $\alpha_{1S}$ or $\beta_{-36}$ subunits because immunolabeling demonstrates a clear presence of both subunits at sites of peripheral couplings (Fig. 2). These findings confirm the critical role of the C-terminal tail of $\beta_{1a}$ subunit in supporting DHPR/

RyR1 communication and indicate that amino acid region encompassing sequence $^{489}$QVQVLTSLRRNLSFW$^{503}$, missing in clone $\beta_{-36}$, contains a determinant of $\beta_{1a}$ that is essential to support skeletal-type EC coupling.

*Disruption of the Hydrophobic Motif Leu$^{496}$-Leu$^{500}$-Trp$^{503}$ Affects EC Coupling Signaling*—The motif conformed by amino acids Leu$^{496}$, Leu$^{500}$, and Trp$^{503}$ of the $\beta_{1a}$ C terminus region has been recently identified in *in vitro* studies as a putative region of interaction with the RyR1 (21). To test whether the absence of residues Leu$^{496}$-Leu$^{500}$-Trp$^{503}$ in our construct $\beta_{-36}$ is directly responsible for the failure of this truncated subunit to restore EC coupling, we designed the construct $\beta_{LLW}$ (Fig. 1). In this clone, residues Leu$^{496}$, Leu$^{500}$, and Trp$^{503}$ were substituted to alanine, a triple mutation that prevented RyR1 activation by peptides derived from the $\beta_{1a}$ C-terminal tail (21). Here we expressed this mutation within the context of construct $\beta_{-14}$ that contains only the critical sequence $^{489}$QVQVLTSLRRNLS-FWGGLEASPR$^{511}$ of the C-terminal domain but that still displays normal EC coupling. The expression of clone $\beta_{LLW}$ in $\beta_1$-null mouse myotubes restored strong depolarization-induced $Ca^{2+}$ release both in the presence and in the absence of extracellular $Ca^{2+}$. However, in comparison with wild type $\beta_{1a}$ and the control clone $\beta_{-14}$, $\beta_{LLW}$-expressing myotubes showed significant reduction in peak $Ca^{2+}$ transient amplitude in response to depolarization (25–30%; Table 1) and an evident rightward shift in $Ca^{2+}$ release sensitivity to depolarization (Fig. 3).

*Truncation of $\beta_{1a}$ C-terminal Tail Amino Acids Gln$^{489}$–Trp$^{503}$ Prevents Organization of the DHPR Complex into Tetrads*—To correlate the effect of $\beta_{1a}$ C-terminal truncations on EC coupling with the structural link between DHPR and RyR1, we also analyzed the ultrastructural organization of the DHPR complex using freeze-fracture electron microscopy. Replicas from myotubes expressing each of the $\beta_{1a}$ constructs displayed numerous small and slightly domed patches of membrane containing clusters of large particles characteristic of DHPR complex (3, 15, 26, 27, 30, 31) (Fig. 4). Myotubes expressing constructs $\beta_{1a}$, $\beta_{-14}$, $\beta_{-21}$, or $\beta_{LLW}$ displayed DHPR particles arranged in arrays of complete and incomplete tetrads that followed an overall orthogonal alignment. In contrast, DHPR particles in $\beta_{-36}$-expressing myotubes were loosely arranged, and no tetrads were present, an arrangement similar to that seen either in dyspedic myotubes that lack RyRs (27) or in $\beta_{1a}$-null zebrafish (17). Table 2 shows counts of all large particles, presumably representing DHPR complexes, within identified membrane patches. Although DHPR particles in myotubes expressing $\beta_{1a}$, $\beta_{-14}$, $\beta_{-21}$, and $\beta_{LLW}$ are clustered at comparable densities, the density is ~50% lower in $\beta_{-36}$ myotubes with no tetrads evident. The combined immunolabeling and freeze-fracture analyzes demonstrate the presence of $\alpha_{1S}/\beta_{-36}$ complexes at peripheral couplings, confirming that the negative results with $\beta_{-36}$ construct are not due to lack of expression or targeting of the DHPR complex to the surface membrane. In addition, the data also reveal that disruption of the Leu$^{496}$-Leu$^{500}$-Trp$^{503}$ motif of $\beta_{1a}$ does not significantly affect the DHPR/RyR1 structural link responsible for the arrangement of DHPR into tetrads.

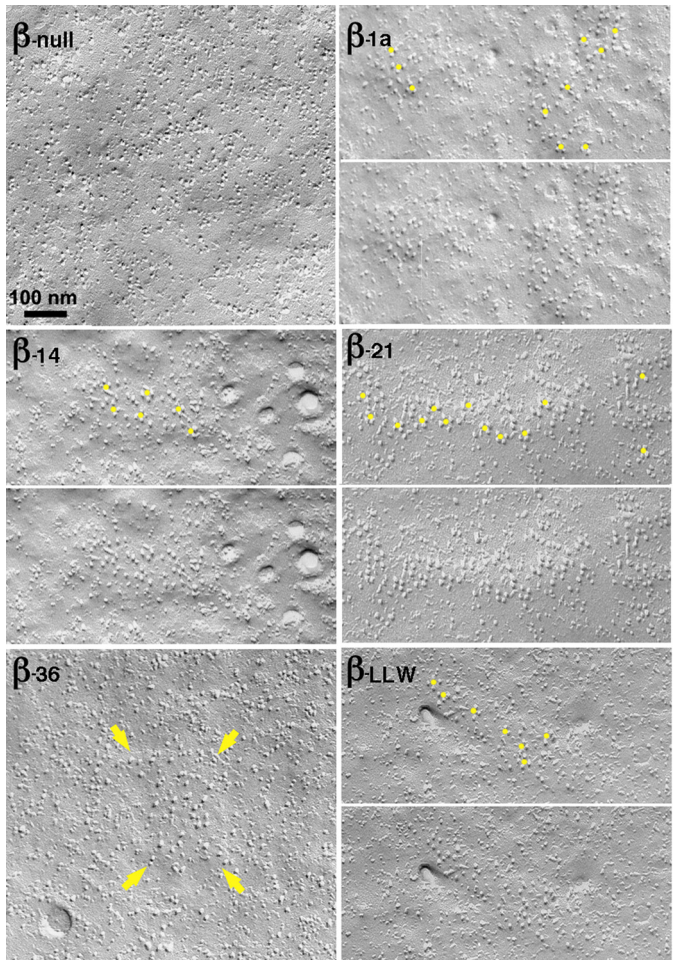


FIGURE 4. **Effect of $\beta_{1a}$ C-terminal truncations on the assembly of DHPR tetrads.** Freeze-fracture replica images showing examples of particle arrangements within the plasmalemma at sites of peripheral couplings in $\beta_1$-null cells expressing various $\beta$ subunits. Intramembranous particle distribution in the $\beta_1$-null cells is completely random. In all cells expressing $\beta$ subunits, a small raised platform caused by the apposition of a junctional SR element to the plasmalemma identifies the position of peripheral couplings. $\beta_{1a}$, $\beta_{-14}$, $\beta_{-21}$, and $\beta_{LLW}$ rescue the formation of DHPR tetrads, whose center is indicated by a *yellow dot* in a duplicate of each image. Tetrad formation, even if somewhat incomplete because of a limited level of expression, indicates that the normal stereospecific association of DHPR with RyR1 is re-established. On the contrary, the few large particles representing the location of DHPRs at a peripheral coupling (indicated by *arrows*) in a $\beta_{-36}$ cell are randomly disposed, indicating a lack of specific DHPR to RyR association.

**TABLE 2**

**Relative density of freeze fracture particle within the junctional membrane**

The values are the means ± S.E. pp, presumably particles representing DHPRs.

| Construct | No. of pp/patch (mean ± S.D.) | Full tetrads/pp |
|---|---|---|
| $\beta_{1a}$ | 30.0 ± 11.6 | 0.11 ± 0.06 |
| $\beta_{-14}$ | 29.3 ± 11.2 | 0.13 ± 0.05 |
| $\beta_{-21}$ | 29.0 ± 13.4 | 0.12 ± 0.07 |
| $\beta_{-36}$ | 14.4 ± 5.0[a] | 0.01 ± 0.02 |
| $\beta_{LLW}$ | 33.6 ± 11.6 | 0.10 ± 0.04 |

[a] $p < 0.05$, compared with $\beta_{1a}$.

*$\beta_{1a}$ C-terminal Truncation of Amino Acids Gln$^{489}$–Trp$^{503}$ Reduces L-type $Ca^{2+}$ Currents*—The effects of $\beta_{1a}$ truncations on $Ca^{2+}$ channel function of the DHPR complex were assessed using whole cell patch clamp analysis. Fig. 5 shows representative traces of $Ca^{2+}$ currents and voltage dependence of the peak

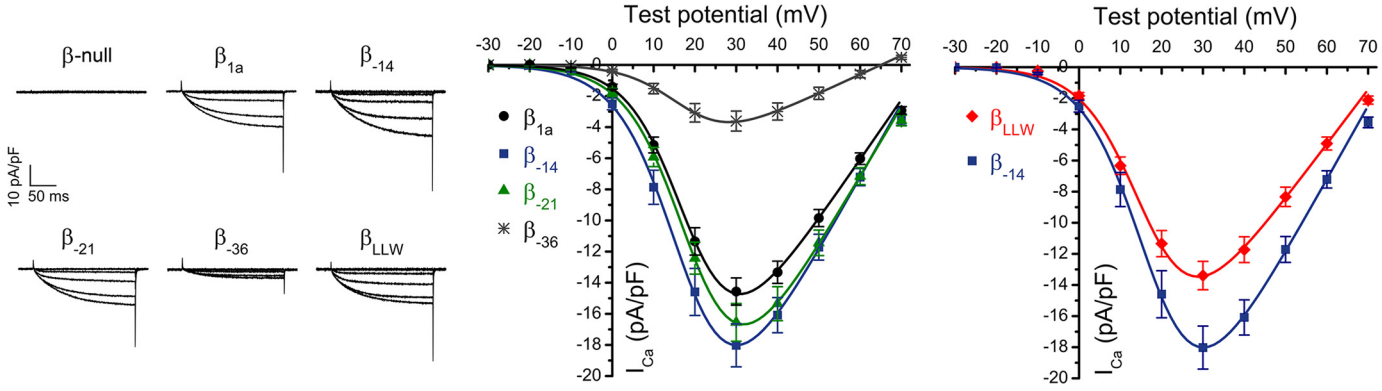


FIGURE 5. **$\beta_{1a}$ C-terminal truncation reduces L-type $Ca^{2+}$ current density.** *Left panel*, representative traces of whole cell $Ca^{2+}$ currents of $\beta_1$-null myotubes expressing the indicated $\beta_{1a}$ constructs. Myotubes were depolarized for 200 ms from a holding potential of −50 mV to test potentials between −40 and +90 mV applied in 10-mV increments. Test sweeps from −20 to +30 mV are shown. *Middle panel*, comparison of voltage dependence of peak $Ca^{2+}$ current densities recorded from $\beta_1$-null myotubes expressing either wild type $\beta_{1a}$ (*black circles*), $\beta_{-14}$ (*blue squares*), $\beta_{-21}$ (*green triangles*), and $\beta_{-36}$ (*gray asterisks*). *Right panel*, the same data from $\beta_1$-null myotubes expressing $\beta_{-14}$ (*blue squares*) is compared with $\beta_1$-null myotubes expressing $\beta_{LLW}$ subunit (*red diamonds*). The *I/V* relationships were fitted using Equation 1 (see "Experimental Procedures"). Fitting parameters for each plot between −40 and +90 mV are presented in Table 3. The data are expressed as means ± S.E., $n = 3$ independent experiments.

**TABLE 3**

**$Ca^{2+}$ conductance and charge movement parameters of myotubes expressing $\beta_{1a}$ C-terminal truncations**

The values were derived by one-way analysis of variance (Tukey's test). The data are presented as means ± S.E. of Boltzman parameters fitted between −30 and +90 mV.

| | *G-V* curves | | | *Q-V* curves | | |
|---|---|---|---|---|---|---|
| | $G_{max}$ | $V_{½}$ | $k$ | $Q_{max}$ | $V_{½}$ | $k$ |
| | *pS/pF* | *mV* | *mV* | *nC/μF* | *mV* | *mV* |
| $\beta_{1a}$ | 301 ± 14 (31) | 17.6 ± 0.7 (31) | 5.6 ± 0.1 (31) | 4.9 ± 0.3 (11) | 13.7 ± 0.8 (11) | 12.6 ± 0.3 (11) |
| $\beta_{-14}$ | 363 ± 23 (23) | 16.4 ± 0.9 (23) | 5.8 ± 0.2 (23) | 4.6 ± 0.9 (6) | 13.2 ± 1.2 (6) | 10.8 ± 0.7 (6) |
| $\beta_{-21}$ | 341 ± 22 (20) | 17.8 ± 0.6 (20) | 6.0 ± 0.1 (20) | 5.4 ± 0.5 (7) | 14.1 ± 1.6 (7) | 12.7 ± 0.7 (7) |
| $\beta_{-36}$ | 105 ± 13 (26)[a] | 18.8 ± 0.9 (26) | 6.1 ± 0.2 (26) | 4.9 ± 0.6 (8) | 9.7 ± 1.9 (8) | 14.7 ± 0.3 (8) |
| $\beta_{LLW}$ | 274 ± 17 (27)[b] | 14.8 ± 0.7 (27) | 5.7 ± 0.1 (27) | 4.6 ± 0.5 (9) | 11.7 ± 1.0 (9) | 14.4 ± 0.6 (9) |

[a] $p < 0.001$, compared with $\beta_{1a}$.
[b] $p < 0.01$, compared with $\beta_{-14}$.

$Ca^{2+}$ current measured in $\beta_1$-null myotubes expressing each of the $\beta$-truncated constructs. $\beta_1$-null myotubes had marginal to nondetectable whole cell $Ca^{2+}$ currents in response to depolarization (Fig. 5, *left panel*). In contrast, $\beta_{1a}$-expressing myotubes showed high density $Ca^{2+}$ currents with slow activation kinetics and fast deactivation, characteristic of L-type $Ca^{2+}$ channels (1, 28, 32). Overall $Ca^{2+}$ current density, maximal conductance ($G_{max}$), and other Boltzmann parameters recorded in myotubes expressing wild type $\beta_{1a}$ subunit (Table 3) were similar to those reported previously by other groups (2, 33–36).

Expression of constructs $\beta_{-14}$, $\beta_{-21}$, and $\beta_{LLW}$ in $\beta_1$-null myotubes rescued high density $Ca^{2+}$ currents similar to $\beta_{1a}$ (Fig. 5). By contrast, myotubes expressing construct $\beta_{-36}$ displayed significantly reduced $Ca^{2+}$ current density (Fig. 5, *middle panels*). Under our experimental conditions, the average peak $Ca^{2+}$ current density displayed by construct $\beta_{-14}$ appeared slightly higher than the one in $\beta_{1a}$-expressing myotubes. However, further analysis revealed no significant difference in $Ca^{2+}$ conductance ($G_{max}$) values between these two clones (Table 3). Likewise, longer deletion $\beta_{-21}$ or mutation of the $Leu^{496}$-$Leu^{500}$-$Trp^{503}$ motif (construct $\beta_{LLW}$) did not result in significant differences in maximal $Ca^{2+}$ current (Fig. 5, *middle* and *right panels*) or $G_{max}$ (Table 3) when compared with $\beta_{1a}$-expressing myotubes. However, $Ca^{2+}$ current density in $\beta_{LLW}$-expressing cells was ~25% smaller than the $Ca^{2+}$ current recovered by cells expressing the control construct $\beta_{-14}$ (Fig. 5, *right panel*). Consistently, an equivalent difference in average $G_{max}$ was observed between these two clones ($p < 0.01$; Table 3). Deletion of the last 36 amino acids of $\beta_{1a}$ C-terminal tail ($\beta_{-36}$), on the other hand, resulted in a severe reduction in peak $Ca^{2+}$ current (Fig. 5, *left* and *middle panels*). Comparison of $Ca^{2+}$ conductance revealed a reduction in average $G_{max}$ of ~65% from 301 ± 14 pS/pF in $\beta_{1a}$-expressing myotubes to 105 ± 13 pS/pF in myotubes expressing $\beta_{-36}$ (Table 3). This $G_{max}$ value is fully consistent with the $Ca^{2+}$ conductance previously reported for a $\beta_{1a}$ construct lacking 35 amino acids of the C-terminal region (88 pS/pF) (18). Further analysis of the recovered $Ca^{2+}$ current indicates that truncation of the $\beta_{1a}$ C-terminal tail or mutational substitution of the $Leu^{496}$-$Leu^{500}$-$Trp^{503}$ motif resulted in no detectable alterations of the $Ca^{2+}$ current kinetics (data not shown). These results suggest that a loss of depolarization-induced $Ca^{2+}$ release signal in myotubes expressing truncation $\beta_{-36}$ is associated with a severe reduction of retrograde signaling from RyR1, as expected for a mutant that do not support tetrad formation (Table 2).

*Truncation of $\beta_{1a}$ C-terminal Tail Does Not Affect Intramembrane Charge Movement*—Immobilization-resistant intramembrane charge movement is a measure of DHPR voltage sensor density. Fig. 6 shows charge *versus* voltage relationships for the five tested constructs obtained by integration of the ON component. Wild type and mutant $\beta_{1a}$-expressing myotubes presented maximal charge movement ($Q_{max}$) and other Boltzmann parameters (Table 3) similar to those reported by others groups (5, 18, 37, 38). The average $Q_{max}$ values measured in myotubes

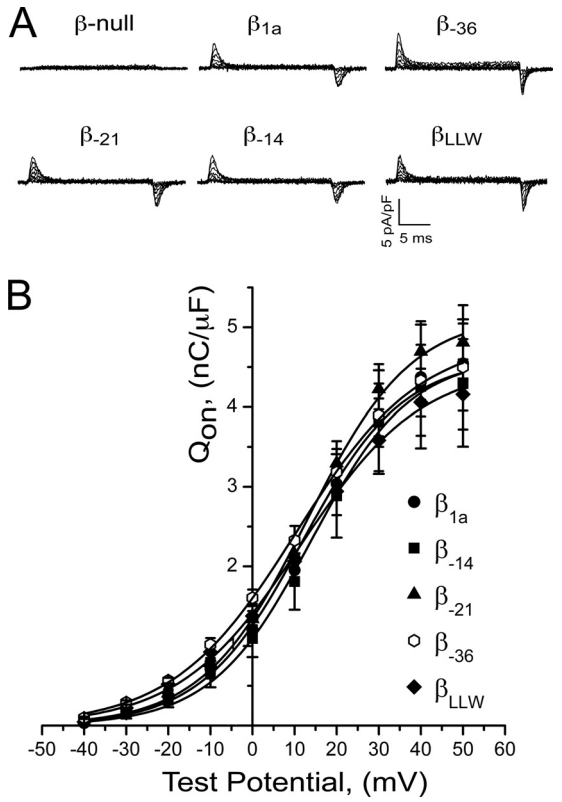


FIGURE 6. **Truncation of the C-terminal tail of $\beta_{1a}$ does not affect DHPR charge movement.** *A*, representative charge movement (*Q*) recording in response to 20-ms depolarizing test pulses between −40 and +50 mV from a holding potential of −50 mV. Test sweeps from −30 to +40 mV are shown. *B*, comparison of voltage dependence of the integrated outward gating current ($Q_{on}$) recorded from $\beta_1$-null myotubes expressing either wild type $\beta_{1a}$ (*circles*), $\beta_{-14}$ (*squares*), $\beta_{-21}$ (*triangles*), $\beta_{-36}$ (*hexagons*), or $\beta_{LLW}$ subunit (*diamonds*). The *Q/V* relationships were fitted to Equation 2, and the parameters are summarized in Table 3. The data are expressed as the means ± S.E., $n = 3$ independent experiments.

expressing the different truncated $\beta_{1a}$ or mutated $\beta_{LLW}$ subunits were not significantly different from the $Q_{max}$ values observed in wild type $\beta_{1a}$-expressing cells (Fig. 6 and Table 3). Therefore, truncations or mutation of the Leu$^{496}$-Leu$^{500}$-Trp$^{503}$ motif of $\beta_{1a}$ did not affect either the voltage-sensing properties of the DHPR or the trafficking and density of the DHPR-$\alpha_{1S}$ subunit to the cell surface.

## DISCUSSION

The essential role of DHPR-$\beta_{1a}$ subunit in EC coupling signaling of skeletal muscle cells is supported by compelling evidence (18, 19, 37, 39, 40), yet the molecular determinant(s) involved in this process are still undefined. In this study, using progressive truncations of the C-terminal region of mouse $\beta_{1a}$ subunit, we found that the domain encompassing amino acid residues Gln$^{489}$–Trp$^{503}$ plays an essential role in supporting bidirectional signaling between the DHPR complex and RyR1 in cultured myotubes. Deletion of this region resulted in a loss of depolarization-induced $Ca^{2+}$ release signal, a severe reduction of L-type $Ca^{2+}$ currents (retrograde signal), and the loss of DHPR organization into arrays of tetrads despite seemingly normal expression and targeting of the DHPR complex to the junctional couplings. These results are fully consistent with work from zebrafish $\beta_1$-null mutant model showing that the lack of expression of $\beta_{1a}$ subunit precludes the skeletal muscle-specific arrangement of DHPR particles into arrays of tetrads, resulting in a loss of EC coupling (16, 17). Thus, our data demonstrate that, like the II-III loop of $\alpha_{1S}$, the $\beta_{1a}$ C terminus constitutes an essential physical and functional link between the DHPR and RyR1.

Whether the loss of a structural link between DHPR and RyR1 by deletion of the Gln$^{489}$–Trp$^{503}$ sequence of $\beta_{1a}$ is the direct result of disruption of a yet unidentified $\beta_{1a}$-RyR1 interaction is unknown. Currently, the strongest evidence supporting a direct link between $\beta_{1a}$ and RyR1 comes primarily from reports of *in vitro* interactions. Previous co-immunoprecipitation studies defined a cluster of positively charged amino acids within domain 3490–3523 of RyR1 as a $\beta_{1a}$-binding domain (41). The disruption of this region not only prevents $\beta_{1a}$-RyR1 interactions *in vitro* but also weakens electrically evoked $Ca^{2+}$ release signals in cultured myotubes (41). Interestingly, $\beta_{1a}$ peptides from the same C-terminal region identified in our study were found to activate native and purified RyR1 channels fused into lipid bilayers (20, 21). Moreover, microinjection of these peptides into flexor digitorum brevis fibers was reported to specifically enhance depolarization-induced $Ca^{2+}$ release (42), further supporting the idea that the C-terminal domain of $\beta_{1a}$ subunit directly interacts with RyR1 and that this interaction is involved in EC coupling signaling. More recently, extensive mutagenesis analysis has found that the active motif in these peptides are residues Leu$^{496}$-Leu$^{500}$-Trp$^{503}$ because alanine substitutions at these positions completely eliminate the activating properties of the peptides (21). In the present study, we show that similar disruption of the Leu$^{496}$-Leu$^{500}$-Trp$^{503}$ motif by site-directed mutagenesis did not abolish depolarization-induced $Ca^{2+}$ release, providing strong indication that the amino acid residues Leu$^{496}$, Leu$^{500}$, and Trp$^{503}$ are not essential for EC coupling. Nonetheless, our data indicate that alanine substitution of these residues significantly affects the efficiency and voltage sensitivity of the EC coupling signal. These changes were linked to a small but statistically significant reduction in $G_{max}$ of the DHPR complex, suggesting an influence of the Leu$^{496}$-Leu$^{500}$-Trp$^{503}$ motif on channel conductance. Thus, although not essential, the Leu$^{496}$-Leu$^{500}$-Trp$^{503}$ motif appears to contribute, to some extent, to the structural determinant of $\beta_{1a}$ subunit that modulates bidirectional signaling in muscle cells.

Previous studies have demonstrated a close correlation between DHPR positioning into tetrads and EC coupling (15, 26, 27), and the data from this study further confirm these findings. Nonetheless, because of the effects of C-terminal truncations of $\beta_{1a}$ ($\beta_{-36}$) on both DHPR current density and SR $Ca^{2+}$ release, we cannot completely rule out a direct involvement of $\beta_{1a}$ on signal transduction between the DHPR and RyR1. However, the severe reduction in $G_{max}$ of the DHPR complex associated with $\beta_{1a}$ truncation is suggestive of an important conformational alteration of the ion-conducting channel, the $\alpha_{1S}$ subunit. Thus, our data seem to be consistent with the hypothesis that $\beta_{1a}$ functions as an allosteric modulator of the $\alpha_{1S}$ subunit, restoring the functional conformation that enables $\alpha_{1S}$ both proper anchorage to RyR1 enabling organization into tetrads and normal channel conductive properties (16, 39).

Recent studies in muscle cells from zebrafish $\beta_{1a}$-null mutant have reported that domain cooperativity between a conserve proline-rich motif at the C-terminal tail ($^{464}$P*XX*P$^{467}$) and the Src homology 3 (SH3) domain of $\beta_{1a}$ are essential to restore the voltage sensing properties of the DHPR complex and, thus, EC coupling signaling (39). Whether similar domain cooperativity is required in mouse skeletal EC coupling is unknown. Crystal structure analysis of mammalian DHPR $\beta_{2a}$ and $\beta_3$ subunits indicates that the SH3 domain would not be compatible with canonical modes of proline-rich ligand binding (43, 44), suggesting that direct interaction between the SH3 domain and $^{464}$P*XX*P$^{467}$ motif of $\beta_{1a}$ would be unlikely. Interestingly, all truncated $\beta_{1a}$ subunits tested in our study, including those that do not support skeletal EC coupling, had an intact $^{464}$P*XX*P$^{467}$ motif. This finding suggests that either domain cooperativity mediated by the P*XX*P motif is not essential for mammalian EC coupling or that in addition to the $^{464}$P*XX*P$^{467}$ motif, other determinant(s) of the C-terminal region, like the one identified in this study, would also be required for functional domain cooperativity.

Overall, our work defines the region of the $\beta_{1a}$ subunit encompassing amino acids $^{489}$QVQVLTSLRRNLSFW$^{503}$ as an essential structural determinant for the physical and functional communication between DHPR complex and the RyR1. The putative $\beta_{1a}$/RyR1-interacting motif Leu$^{496}$-Leu$^{500}$-Trp$^{503}$ enclosed within this segment influences the efficiency of EC coupling signal, but it appears to be not essential for either DHPR-RyR1 bidirectional signaling or DHPR tetrad organization.

*Acknowledgment—We thank Dr. J. Fessenden for critical reading of the manuscript.*

## REFERENCES


1. Grabner, M., Dirksen, R. T., Suda, N., and Beam, K. G. (1999) The II–III loop of the skeletal muscle dihydropyridine receptor is responsible for the bi-directional coupling with the ryanodine receptor. *J. Biol. Chem.* **274,** 21913–21919
2. Nakai, J., Dirksen, R. T., Nguyen, H. T., Pessah, I. N., Beam, K. G., and Allen, P. D. (1996) Enhanced dihydropyridine receptor channel activity in the presence of ryanodine receptor. *Nature* **380,** 72–75
3. Takekura, H., Bennett, L., Tanabe, T., Beam, K. G., and Franzini-Armstrong, C. (1994) Restoration of junctional tetrads in dysgenic myotubes by dihydropyridine receptor cDNA. *Biophys. J.* **67,** 793–803
4. Beam, K. G., Knudson, C. M., and Powell, J. A. (1986) A lethal mutation in mice eliminates the slow calcium current in skeletal muscle cells. *Nature* **320,** 168–170
5. Beurg, M., Sukhareva, M., Strube, C., Powers, P. A., Gregg, R. G., and Coronado, R. (1997) Recovery of $Ca^{2+}$ current, charge movements, and $Ca^{2+}$ transients in myotubes deficient in dihydropyridine receptor $\beta$1 subunit transfected with $\beta$1 cDNA. *Biophys. J.* **73,** 807–818
6. Chaudhari, N., and Beam, K. G. (1989) The muscular dysgenesis mutation in mice leads to arrest of the genetic program for muscle differentiation. *Dev. Biol.* **133,** 456–467
7. Coronado, R., Ahern, C. A., Sheridan, D. C., Cheng, W., Carbonneau, L., and Bhattacharya, D. (2004) Functional equivalence of dihydropyridine receptor $\alpha$1S and $\beta$1a subunits in triggering excitation-contraction coupling in skeletal muscle. *Biol. Res.* **37,** 565–575
8. Flucher, B. E., Obermair, G. J., Tuluc, P., Schredelseker, J., Kern, G., and Grabner, M. (2005) The role of auxiliary dihydropyridine receptor subunits in muscle. *J. Muscle Res. Cell Motil.* **26,** 1–6
9. Gregg, R. G., Messing, A., Strube, C., Beurg, M., Moss, R., Behan, M., Sukhareva, M., Haynes, S., Powell, J. A., Coronado, R., and Powers, P. A. (1996) Absence of the $\beta$ subunit (cchb1) of the skeletal muscle dihydropyridine receptor alters expression of the $\alpha$1 subunit and eliminates excitation-contraction coupling. *Proc. Natl. Acad. Sci. U.S.A.* **93,** 13961–13966
10. Knudson, C. M., Chaudhari, N., Sharp, A. H., Powell, J. A., Beam, K. G., and Campbell, K. P. (1989) Specific absence of the $\alpha$1 subunit of the dihydropyridine receptor in mice with muscular dysgenesis. *J. Biol. Chem.* **264,** 1345–1348
11. Tanabe, T., Beam, K. G., Powell, J. A., and Numa, S. (1988) Restoration of excitation-contraction coupling and slow calcium current in dysgenic muscle by dihydropyridine receptor complementary DNA. *Nature* **336,** 134–139
12. Ahern, C. A., Arikkath, J., Vallejo, P., Gurnett, C. A., Powers, P. A., Campbell, K. P., and Coronado, R. (2001) Intramembrane charge movements and excitation-contraction coupling expressed by two-domain fragments of the Ca2+ channel. *Proc. Natl. Acad. Sci. U.S.A.* **98,** 6935–6940
13. Nakai, J., Tanabe, T., Konno, T., Adams, B., and Beam, K. G. (1998) Localization in the II-III loop of the dihydropyridine receptor of a sequence critical for excitation-contraction coupling. *J. Biol. Chem.* **273,** 24983–24986
14. Nakai, J., Ogura, T., Protasi, F., Franzini-Armstrong, C., Allen, P. D., and Beam, K. G. (1997) Functional nonequality of the cardiac and skeletal ryanodine receptors. *Proc. Natl. Acad. Sci. U.S.A.* **94,** 1019–1022
15. Takekura, H., Paolini, C., Franzini-Armstrong, C., Kugler, G., Grabner, M., and Flucher, B. E. (2004) Differential contribution of skeletal and cardiac II–III loop sequences to the assembly of dihydropyridine-receptor arrays in skeletal muscle. *Mol. Biol. Cell* **15,** 5408–5419
16. Schredelseker, J., Dayal, A., Schwerte, T., Franzini-Armstrong, C., and Grabner, M. (2009) Proper restoration of excitation-contraction coupling in the dihydropyridine receptor $\beta$1-null zebrafish relaxed is an exclusive function of the $\beta$1a subunit. *J. Biol. Chem.* **284,** 1242–1251
17. Schredelseker, J., Di Biase, V., Obermair, G. J., Felder, E. T., Flucher, B. E., Franzini-Armstrong, C., and Grabner, M. (2005) The $\beta$1a subunit is essential for the assembly of dihydropyridine-receptor arrays in skeletal muscle. *Proc. Natl. Acad. Sci. U.S.A.* **102,** 17219–17224
18. Beurg, M., Ahern, C. A., Vallejo, P., Conklin, M. W., Powers, P. A., Gregg, R. G., and Coronado, R. (1999) Involvement of the carboxy-terminus region of the dihydropyridine receptor $\beta$1a subunit in excitation-contraction coupling of skeletal muscle. *Biophys. J.* **77,** 2953–2967
19. Sheridan, D. C., Cheng, W., Ahern, C. A., Mortenson, L., Alsammarae, D., Vallejo, P., and Coronado, R. (2003) Truncation of the carboxyl terminus of the dihydropyridine receptor $\beta$1a subunit promotes Ca2+ dependent excitation-contraction coupling in skeletal myotubes. *Biophys. J.* **84,** 220–237
20. Rebbeck, R. T., Karunasekara, Y., Gallant, E. M., Board, P. G., Beard, N. A., Casarotto, M. G., and Dulhunty, A. F. (2011) The $\beta$(1a) subunit of the skeletal DHPR binds to skeletal RyR1 and activates the channel via its 35-residue C-terminal tail. *Biophys. J.* **100,** 922–930
21. Karunasekara, Y., Rebbeck, R. T., Weaver, L. M., Board, P. G., Dulhunty, A. F., and Casarotto, M. G. (2012) An $\alpha$-helical C-terminal tail segment of the skeletal L-type $Ca^{2+}$ channel $\beta$1a subunit activates ryanodine receptor type 1 via a hydrophobic surface. *Faseb J.* **26,** 5049–5059
22. Lee, D. Y., and Sugden, B. (2008) The LMP1 oncogene of EBV activates PERK and the unfolded protein response to drive its own synthesis. *Blood* **111,** 2280–2289
23. Westerman, K. A., Penvose, A., Yang, Z., Allen, P. D., and Vacanti, C. A. (2010) Adult muscle "stem" cells can be sustained in culture as free-floating myospheres. *Exp. Cell Res.* **316,** 1966–1976
24. Eltit, J. M., Li, H., Ward, C. W., Molinski, T., Pessah, I. N., Allen, P. D., and Lopez, J. R. (2011) Orthograde dihydropyridine receptor signal regulates ryanodine receptor passive leak. *Proc. Natl. Acad. Sci. U.S.A.* **108,** 7046–7051
25. Sheridan, D. C., Takekura, H., Franzini-Armstrong, C., Beam, K. G., Allen, P. D., and Perez, C. F. (2006) Bidirectional signaling between calcium channels of skeletal muscle requires multiple direct and indirect interactions. *Proc. Natl. Acad. Sci. U.S.A.* **103,** 19760–19765
26. Paolini, C., Protasi, F., and Franzini-Armstrong, C. (2004) The relative

position of RyR feet and DHPR tetrads in skeletal muscle. *J. Mol. Biol.* **342,** 145–153
27. Protasi, F., Franzini-Armstrong, C., and Allen, P. D. (1998) Role of ryanodine receptors in the assembly of calcium release units in skeletal muscle. *J. Cell Biol.* **140,** 831–842
28. García, J., and Beam, K. G. (1994) Measurement of calcium transients and slow calcium current in myotubes. *J. Gen. Physiol.* **103,** 107–123
29. Adams, B. A., Tanabe, T., Mikami, A., Numa, S., and Beam, K. G. (1990) Intramembrane charge movement restored in dysgenic skeletal muscle by injection of dihydropyridine receptor cDNAs. *Nature* **346,** 569–572
30. Protasi, F., Franzini-Armstrong, C., and Flucher, B. E. (1997) Coordinated incorporation of skeletal muscle dihydropyridine receptors and ryanodine receptors in peripheral couplings of BC3H1 cells. *J. Cell Biol.* **137,** 859–870
31. Takekura, H., Nishi, M., Noda, T., Takeshima, H., and Franzini-Armstrong, C. (1995) Abnormal junctions between surface membrane and sarcoplasmic reticulum in skeletal muscle with a mutation targeted to the ryanodine receptor. *Proc. Natl. Acad. Sci. U.S.A.* **92,** 3381–3385
32. García, J., Tanabe, T., and Beam, K. G. (1994) Relationship of calcium transients to calcium currents and charge movements in myotubes expressing skeletal and cardiac dihydropyridine receptors. *J. Gen. Physiol.* **103,** 125–147
33. Avila, G., and Dirksen, R. T. (2005) Rapamycin and FK506 reduce skeletal muscle voltage sensor expression and function. *Cell Calcium* **38,** 35–44
34. Gach, M. P., Cherednichenko, G., Haarmann, C., Lopez, J. R., Beam, K. G., Pessah, I. N., Franzini-Armstrong, C., and Allen, P. D. (2008) $\alpha 2\delta 1$ dihydropyridine receptor subunit is a critical element for excitation-coupled calcium entry but not for formation of tetrads in skeletal myotubes. *Biophys. J.* **94,** 3023–3034
35. Avila, G., O'Connell, K. M., Groom, L. A., and Dirksen, R. T. (2001) $Ca^{2+}$ release through ryanodine receptors regulates skeletal muscle L-type $Ca^{2+}$ channel expression. *J. Biol. Chem.* **276,** 17732–17738
36. Bannister, R. A., Estève, E., Eltit, J. M., Pessah, I. N., Allen, P. D., López, J. R., and Beam, K. G. (2010) A malignant hyperthermia-inducing mutation in RYR1 (R163C): consequent alterations in the functional properties of DHPR channels. *J. Gen. Physiol.* **135,** 629–640
37. Sheridan, D. C., Cheng, W., Carbonneau, L., Ahern, C. A., and Coronado, R. (2004) Involvement of a heptad repeat in the carboxyl terminus of the dihydropyridine receptor $\beta 1$a subunit in the mechanism of excitation-contraction coupling in skeletal muscle. *Biophys. J.* **87,** 929–942
38. Sheridan, D. C., Moua, O., Lorenzon, N. M., and Beam, K. G. (2012) Bimolecular fluorescence complementation and targeted biotinylation provide insight into the topology of the skeletal muscle $Ca^{2+}$ channel $\beta 1$a subunit. *Channels* **6,** 26–40
39. Dayal, A., Bhat, V., Franzini-Armstrong, C., and Grabner, M. (2013) Domain cooperativity in the $\beta 1$a subunit is essential for dihydropyridine receptor voltage sensing in skeletal muscle. *Proc. Natl. Acad. Sci. U.S.A.* **110,** 7488–7493
40. Dayal, A., Schredelseker, J., Franzini-Armstrong, C., and Grabner, M. (2010) Skeletal muscle excitation-contraction coupling is independent of a conserved heptad repeat motif in the C-terminus of the DHPR$\beta$(1a) subunit. *Cell Calcium* **47,** 500–506
41. Cheng, W., Altafaj, X., Ronjat, M., and Coronado, R. (2005) Interaction between the dihydropyridine receptor $Ca^{2+}$ channel $\beta$_subunit and ryanodine receptor type 1 strengthens excitation-contraction coupling. *Proc. Natl. Acad. Sci. U.S.A.* **102,** 19225–19230
42. Hernández-Ochoa, E. O., Olojo, R. O., Rebbeck, R. T., Dulhunty, A. F., and Schneider, M. F. (2014) $\beta 1$a490-508, a 19-residue peptide from C-terminal tail of Cav1.1 $\beta 1$a subunit, potentiates voltage-dependent calcium release in adult skeletal muscle fibers. *Biophys. J.* **106,** 535–547
43. Chen, Y. H., Li, M. H., Zhang, Y., He, L. L., Yamada, Y., Fitzmaurice, A., Shen, Y., Zhang, H., Tong, L., and Yang, J. (2004) Structural basis of the $\alpha 1$-$\beta$ subunit interaction of voltage-gated $Ca^{2+}$ channels. *Nature* **429,** 675–680
44. Van Petegem, F., Clark, K. A., Chatelain, F. C., and Minor, D. L., Jr. (2004) Structure of a complex between a voltage-gated calcium channel $\beta$_subunit and an $\alpha$-subunit domain. *Nature* **429,** 671–675